



RESEARCH ARTICLE | FEBRUARY 13 2024

# The effect of In(Ga)As/GaAs quantum dots on the optical loss of photonic crystal cavities

Matteo Lodde ; Rene P. J. van Veldhoven ; Ewold Verhagen ; Andrea Fiore 




*J. Appl. Phys.* 135, 063103 (2024)


<https://doi.org/10.1063/5.0189904>



CrossMark




Lock-in Amplifier



Boxcar Averager

Boost Your Optics and Photonics Measurements

 Zurich Instruments

[Find out more](#)

# The effect of In(Ga)As/GaAs quantum dots on the optical loss of photonic crystal cavities

Cite as: J. Appl. Phys. 135, 063103 (2024); doi: 10.1063/5.0189904

Submitted: 1 December 2023 · Accepted: 19 January 2024 ·

Published Online: 13 February 2024



Matteo Lodde,<sup>1,a)</sup> Rene P. J. van Veldhoven,<sup>1</sup> Ewold Verhagen,<sup>1,2</sup> and Andrea Fiore<sup>1</sup>

## AFFILIATIONS

<sup>1</sup>Department of Applied Physics and Science Education, Eindhoven Hendrik Casimir Institute, Eindhoven University of Technology, 5612 AZ Eindhoven, The Netherlands

<sup>2</sup>Center for Nanophotonics, AMOLF, Amsterdam, The Netherlands

<sup>a)</sup>Author to whom correspondence should be addressed: [m.lodde@tue.nl](mailto:m.lodde@tue.nl)

## ABSTRACT

We present a systematic investigation of the optical losses in GaAs photonic crystal cavities with and without embedded self-assembled In(Ga)As quantum dots (QDs) to shed light on additional loss mechanisms related to the presence of the QDs. To clarify the role of the measurement method, we propose an experimental configuration where the optical properties can be evaluated simultaneously through reflection and photoluminescence measurements. Independently of the measurement method, we observe a reduced quality (Q) factor in cavities with embedded QDs when compared to the passive counterparts. Our analysis indicates that these additional losses—about 7 GHz—are unrelated to direct excitonic absorption for the investigated areal QD densities of  $175 \mu\text{m}^{-2}$ . We analyze several mechanisms which could explain our observations and suggest that a possible origin could be unsaturable absorption from midgap defects introduced by the QD growth.

© 2024 Author(s). All article content, except where otherwise noted, is licensed under a Creative Commons Attribution (CC BY) license (<http://creativecommons.org/licenses/by/4.0/>). <https://doi.org/10.1063/5.0189904>

## I. INTRODUCTION

Over the past three decades, there has been tremendous interest in light-matter interaction in nanophotonic cavities. Photonic crystal cavities (PhCCs), in particular, have been shown to be suitable for confining light in mode volumes (V) on the order of a cubic wavelength, with high quality (Q) factors on the order of  $10^6$ <sup>1–3</sup> (with a record-high Q in Si reaching  $10^{7.4}$ ) and the highest Q/V ratio.<sup>5</sup> Embedding semiconductors quantum dots (QDs) in these systems allows defining discrete electronic states with the corresponding effective optical nonlinearity. This is very promising for a plethora of applications, such as lasing,<sup>6,7</sup> single photon generation,<sup>8–11</sup> and photonic quantum gates.<sup>12,13</sup> In all these systems, minimizing the loss rate plays a critical role—for example—a coherent excitation swap between an exciton in the QD and a photon in the cavity is possible only if the coupling rate overcomes the loss rate.

However, all reported PhCCs devices with embedded QDs have Q factors that remain few orders of magnitude lower than their passive counterparts, typically around  $10^4$ .<sup>14–17</sup> Effort has been made to reduce the losses by means of surface passivation, which has allowed reaching Qs in the order of  $10^5$  for PhCCs with

In(Ga)As/GaAs QDs.<sup>18</sup> Even so, this figure remains one order of magnitude lower than that of comparable devices without QDs.

Strikingly, despite its relevance, the physical origin of the extra losses is still a subject of debate. Recent studies have highlighted that, for PhCCs, electronic states in the bandgap play a pivotal role.<sup>18</sup> We note that in these works the ground state energy of the QDs ( $\sim 1.35$  eV) and therefore the frequency of the PhCC modes are close to the bandgap of GaAs, making the devices susceptible to band-tail absorption<sup>19</sup> or absorption by shallow defects. PhCCs with  $Q > 10^6$  (without QDs) have indeed only been realized at longer wavelengths. It might be expected that by shifting the QDs' emission to telecom wavelengths (1.3 or 1.55  $\mu\text{m}$ ), it would be possible to couple the QD excitonic levels to PhCC modes with very high Qs, as band-tail effects should be negligible far from the gap. Unfortunately, this is not the case, as Q has remained limited also in this wavelength region,<sup>20</sup> pointing to other sources of loss not yet extensively explored.

The investigation of the loss introduced by QDs involves significant experimental challenges. For example, we note that all the reported studies so far focus on the minimization of the losses in

QD-containing PhCCs, but lack a control measurement in which the same design is fabricated with and without QDs and measured in the same experimental conditions. This raises the question as to whether the observed loss is inherently related to the presence of QDs or rather to the structure and choice of operating wavelengths. An additional uncertainty relates to the experimental method employed to measure  $Q$ . Indeed, samples with embedded QDs are often conveniently studied by means of PL, while high- $Q$  passive devices are characterized in reflection or transmission. Carrier injection, as employed in PL experiments, may produce free-carrier absorption (FCA) losses and therefore affect the  $Q$ -factor measurement. A comparison of the two measurement methods has not been performed to the best of our knowledge.

In this paper, we address these questions by reporting a comprehensive investigation to measure the impact of the presence of self-embedded In(Ga)As/GaAs QDs emitting at  $\sim 1.3\mu\text{m}$  on optical losses in PhCCs. To this end, we conduct a comparative analysis on identical photonic crystal structures fabricated in wafers with and without embedded QDs. First, we observe a systematic difference in loss between the two structures, the QD-PhCCs presenting an additional loss rate of  $\approx 7$  GHz on average. To ascertain whether the additional optical losses are related to direct excitonic absorption, we characterize PhCCs in and out of resonance with respect to the ground state emission of the QDs and observe no significant difference. We compare measurements carried out on QD samples simultaneously in reflection and micro-PL in order to evaluate the role of the experimental technique. Finally, we investigate the impact of carrier injection on the losses of the samples with and without QDs. This systematic set of experiments allows us to conclude that the observed additional loss is not related to direct excitonic absorption or to scattering related to geometrical or compositional inhomogeneities due to the presence of the QDs. Our observations are rather compatible with an additional absorption process related to the presence of midgap states in the QD layer. This indicates the key role of QD growth optimization and suggests a route toward the further improvement of QD nanophotonic devices.

## II. METHODS

### A. Design

The geometry of our PhCC consists of a single nanobeam with elliptical holes,<sup>1</sup> as shown in the simulation on Fig. 1(b). This geometry allows efficiency coupling to an on-chip optical waveguide, enabling reflection measurements. The optical cavity is formed by a gradual change of the hole parameters (size, ellipticity, and lattice constant) between the outer crystal cell and the defect in the center, resulting in a localized optical mode. The parametrization of the gradual change is then numerically optimized by performing FEM simulations (with COMSOL Multiphysics) to maximize the  $Q$  factor of the fundamental optical mode. In order to cover the entire range of the ground state of the QD emission, we optimized five different PhCCs designs, with optical resonances spanning from 1250 to 1350 nm, with simulated unloaded  $Q$  factor in the order of  $10^6$ .

In order to measure in the same experimental condition samples with and without QDs, each nanobeam is side-coupled to a waveguide [in red in Fig. 1(c)]. The waveguide is terminated at

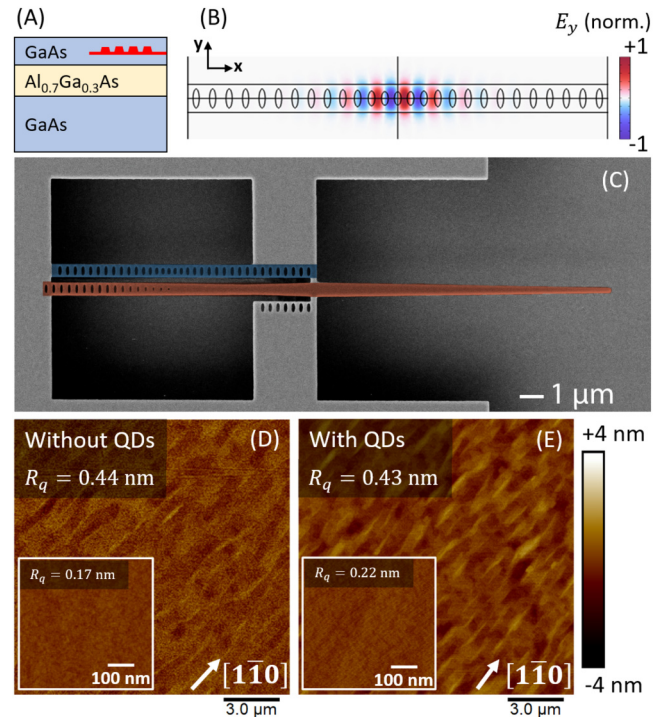


**FIG. 1.** (a) Schematics of the layer stack. The QD layer is indicated in red. (b) Map of the electric field for the fundamental optical mode of one of the designs, with a resonance wavelength tuned to 1295 nm, and a simulated unloaded  $Q$  factor of  $1.5 \times 10^6$ . (c) SEM of one of the fabricated devices. The nanobeam photonic crystal cavity is colored in blue, the side-coupled waveguide in red. (d) and (e) AFM images of the surface of the sample with and without QDs, showing the surface roughness. Insets show a measurement with a higher spatial resolution in a small area, comparable with typical nanobeam dimensions.

the edge of the chip such that it can be coupled to a lensed optical fiber. The tip of the waveguide is 200 nm wide, resulting in an effective mode index close to 1, thus minimizing the backreflections at the air interface at the waveguide termination. The width is adiabatically increased from the tip toward the location of the PhCC to match the effective index of the waveguide to that of the nanobeam there.<sup>21</sup> The waveguide is then terminated on the other side with a photonic crystal mirror having a bandgap centered on the PhCC's resonance wavelength. The coupling rate between the cavity and the waveguide are undercoupled, meaning that the total losses of the system are dominated by the internal losses.

### B. Growth and fabrication

For the study, we grew one wafer with a layer stack consisting of a 250 nm-thick GaAs membrane on top of a  $3\mu\text{m}$ -thick  $\text{Al}_{0.7}\text{Ga}_{0.3}\text{As}$  sacrificial layer that decouples the membrane from the GaAs substrate. Another wafer, with an identical layer stack and nominal thicknesses was grown, integrating a layer of self-assembled

InAs QDs in the middle of the GaAs membrane [see Fig. 1(a)]. The growth was carried out with a molecular-beam epitaxy reactor, and the growth conditions have been tuned to ensure a dot density of  $175\ \mu\text{m}^{-2}$ , confirmed with atomic force microscope (AFM) measurements of uncapped QDs sample, and a room temperature emission at 1280 nm.<sup>22</sup> The relatively high QD density serves to make it easier to assess any effect related to the presence of QDs on the optical loss of PhCCs.

The surface growth temperature of the sacrificial layer and GaAs membrane was 575 °C, as measured by a kSA Bandit band-edge measurement setup. For the QD growth, the temperature was reduced to 480 °C. The InAs QDs were grown with a growth rate of 0.041 Å/s to a thickness of 2.1 monolayers and then annealed for 40 s under As flux only. Finally, the QDs were capped with a 5 nm layer of  $\text{In}_{0.15}\text{Ga}_{0.85}\text{As}$  and a 10 nm thick GaAs layer. The remaining GaAs membrane was grown after heating up to 575 °C. To reduce the surface roughness, the stack was heated up to 600 °C and three monolayers of GaAs were grown followed by a 10 min anneal under As flux only.

Prior to fabrication, both wafers have been characterized to confirm that the membrane thickness is the same within  $\sim 10$  nm (by means of cross-sectional scanning electron microscopy) and surface roughness with atomic force microscope measurements of the surface, as reported in Figs. 1(d) and 1(e). These figures report both a large-area measurement in an area  $15 \times 15\ \mu\text{m}^2$  as well as a small-area measurement of  $500 \times 500\ \text{nm}^2$  in the insets. For both areas, the root mean square roughness ( $R_q$ ) has values lower than 0.5 nm, for both wafers, confirming the efficacy of the annealing procedure used during the growth. We clearly see a twofold increase in roughness in the large area measurements compared to those on small areas, showing that the main contribution to the roughness is given by relatively large hills. Particularly, in Fig. 1(e) we note the presence of shallow mounds elongated along the  $[1\bar{1}0]$  direction, as already reported in the literature for this type of high-density QDs.<sup>23</sup> Any possible effect of such mounds on the loss will be discussed in Sec. IV.

The two samples, with and without QDs, were fabricated together using the same fabrication sequence. Prior to the fabrication steps, the wafer was cleaned with isopropanol and acetone and de-oxidized by using a solution of HCl:H<sub>2</sub>O in a 1:1 ratio for 4 min. Then a 250 nm-thick silicon nitride hard mask was deposited using plasma-enhanced chemical vapor deposition (PECVD). The designed pattern was defined in a ZEP 520A resist by using electron beam lithography. The pattern was transferred first to the silicon nitride hard mask and then to the GaAs membrane using reactive-ion etching. Finally, the sacrificial layer was removed by etching at room temperature for 1 min in a solution of HF 10% in water. Particular attention was given to minimize any fabrication differences between the two samples. To this aim, all the etching steps have been carried out by placing the two samples together in the reaction chambers.

### C. Experimental setup

An experimental setup [schematics in Fig. 2(a)] is employed that allows the simultaneous optical characterization of the PhCCs via photoluminescence and reflection. The samples are placed in a vacuum system, where a lensed fiber controlled by x-y-z piezo

stages is aligned in front of the waveguide. For the reflection measurements we use a fiber-coupled laser tunable in the range of 1260–1360 nm, thus covering the entire ground state emission of the QDs at room temperature. By using a circulator, we send the laser light to the lensed fiber and the reflected light to a photodetector. To ensure good coupling to the waveguide, which supports only a transverse-electric (TE) mode, all the fibers and fiber-coupled devices (up to the lensed fiber) are polarization-maintaining. The reflection measurements are performed by sweeping the laser wavelength and recording the reflected signal. The synchronization between the laser wavelength and the power measured by the photodetector is performed with an oscilloscope which is triggered by a synchronization signal coming from the laser.

The micro-PL part of the setup consists of a cage system held above the sample by a x-y-z piezo stage which allows the alignment of the optical microscopy setup for photoluminescence without moving the sample. As such, we can scan the surface of the device to find the best optical alignment, while keeping the alignment between the lensed fiber and the waveguide fixed. To image the sample for the alignment, the setup includes a red LED as a broad light source and a CCD camera. As a pump source, we use a fiber-coupled continuous-wave (CW) diode laser emitting at 785 nm. The laser light is focused onto the sample using an objective lens (from Mitutoyo, N.A. 0.42, magnification 50 $\times$ ), providing a spot size of about  $8\ \mu\text{m}^2$ . The PL is collected via the same objective. To split the collection and pump paths, we use a dichroic mirror with a cutoff wavelength at 1000 nm. The PL signal is finally coupled to a single-mode fiber connected to a spectrometer [with a Gaussian instrument response function (IRF) characterized by a  $\sigma_{\text{PL}} = 4$  GHz]. All measurements were performed at room temperature.

## III. EXPERIMENTAL RESULTS

### A. Loss analysis in the absence of optical pump

Several PhCCs, whose resonance wavelength ( $\lambda_0$ ) is tuned to cover the whole O-band (1260–1360 nm), were first measured in reflection [Figs. 2(b) and 2(c)]. The total loss rate  $\kappa$  ( $= \lambda_0/cQ$ ) of each cavity is extracted using a Lorentzian fit with a linear background. For these measurements, the power of the tunable laser was attenuated to reduce the optical bistability effect<sup>24</sup> that would affect the measured resonance profile. The amplitude of the reflection dip ( $R_{\text{min}}$ ) in resonance varies among the devices, as it depends on the ratio between intrinsic loss rate ( $\kappa_0$ , influenced by the fabrication imperfections) and the coupling rate to the waveguide (extrinsic loss rate  $\kappa_{\text{ex}}$ , which depends on the distance between the waveguide and the nanobeam) following the relation<sup>25</sup>

$$R_{\text{min}} = |\kappa_0 - \kappa_{\text{ex}}|/\kappa.$$

A comparison of the total loss rates  $\kappa$  of 149 cavities with and without QDs, measured in reflection, is reported in Fig. 3(a). Here we clearly see a consistently higher loss for the cavities with embedded QDs. Indeed, the weighted mean loss rate for the cavities with QDs is  $\bar{\kappa}_{\text{QD}}/2\pi = 16 \pm 1$  GHz (the error is given by the standard deviation of the mean), while for the samples without QDs we get  $\bar{\kappa}_{\text{noQD}}/2\pi = 8.5 \pm 0.3$  GHz. The lowest loss rate measured in the sample without QDs was  $\bar{\kappa}_{\text{noQD}}^{\text{best}}/2\pi = 3.4 \pm 0.3$  GHz ( $Q_{\text{noQD}}^{\text{best}} = 6.8 \times 10^4$ ), in the one with QDs the minimum loss rate

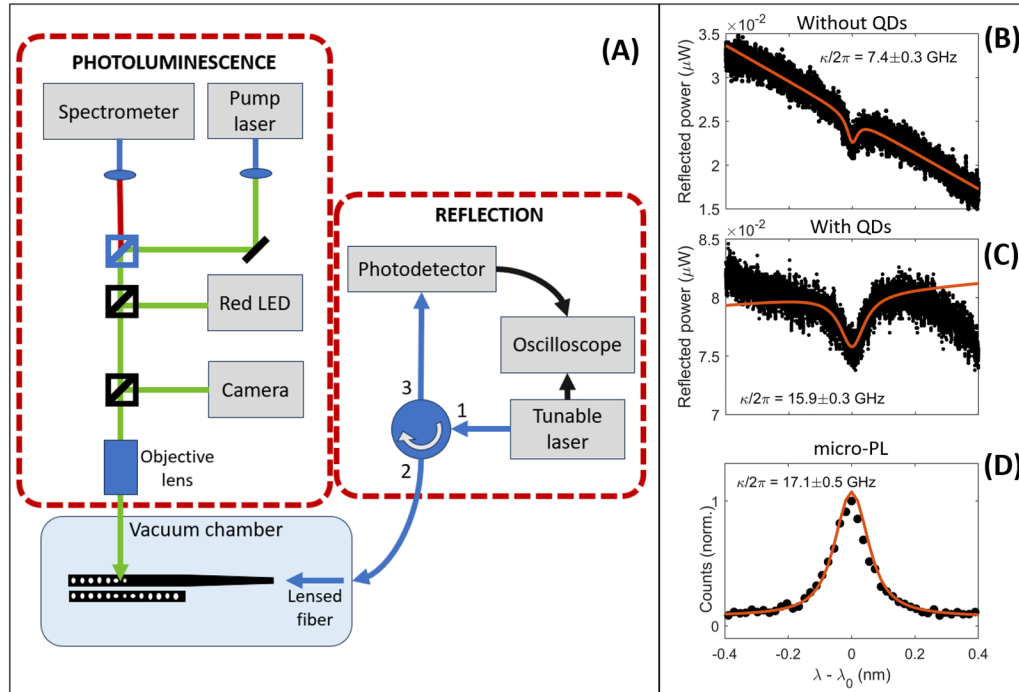


**FIG. 2.** (a) Schematic representation of the experimental setup. Blue lines represent polarization-maintaining optical fibers, while the free space path of the micro-PL setup is indicated in green and red. The black arrows represent the electrical connections. (b) and (c) Reflection measurement of two identical cavities (with same nominal parameters) fabricated without (b) and with (c) QDs, showing the Lorentzian resonance (red fit) of the PhCC. (d) PL measurement of a cavity with QDs [same as the one shown in (c)] with a Voigt fit (red line).

was  $\kappa_{QD}^{best}/2\pi = 8.3 \pm 0.2$  GHz ( $Q_{QD}^{best} = 2.6 \times 10^4$ ). We remark that these values are consistent with what has already been measured in the past in our group on similar cavities in more than 15 fabrication processes, where the highest Qs consistently remained below  $3 \times 10^4$  for cavities with embedded QDs, whereas for samples without QDs we achieved quality factors up to  $7 \times 10^4$ . Even when considering samples without QDs, the reported experimental Qs are about two orders of magnitude smaller than the simulated theoretical values. This discrepancy can be attributed to the fabrication imperfections (e.g., random changes in hole position and radius) and sidewall roughness.

Apart from two outliers at short wavelengths with higher loss rates, no significant increase of the loss is observed for the cavities resonant with the QD ground state (GS) emission. Indeed, the difference of the mean of the losses for cavities at short/long wavelengths (below/above 1300 nm),  $(\kappa_{QD}^{short} - \kappa_{QD}^{long})/2\pi = 3.2$  GHz, is of the same order as their standard deviation, and smaller than the difference between samples with and without QDs. This indicates that the excess loss rate  $(\kappa_{QD} - \kappa_{noQD})/2\pi$  associated to the QDs is not primarily caused by inter-band absorption.

## B. Role of the measurement method

In this section, we study the role of the measurement method in the loss rate estimation, performing PL and reflection

measurement at the same time. We also perform reflection measurements while pumping at 785 nm, to identify any effect due to the carriers created by the pump. For this comparison, we focus on the low pump power regime. An example of PL measurement in this regime is shown in Fig. 2(d). In Sec. III C, we will discuss the effects at higher powers. In order to separate the optical loss rate from the effect of finite spectrometer resolution, we fit the data with a Voigt function, where the Gaussian contribution is kept fixed as it represents the spectrometer response function with  $\sigma_{PL} = 4$  GHz (characterized by measuring the spectrum of an attenuated laser). This way we can deconvolve the intrinsic Lorentzian cavity linewidth from the instrumental response and measure linewidths below the spectrometer resolution.

Figure 3(b) reports the measured data of a cavity with QDs with a resonance wavelength at 1333 nm. This cavity has been chosen as its loss rate is close to the mean value of the entire set of measurement. It is thus expected to be a good representative of the general behavior. In this plot, the points represent the loss rate measured in reflection (black datapoints) and PL (green). The error bars are derived from the fit procedure and are mainly affected by the low signal-to-noise ratio of the PL data taken at such low powers. The plot shows comparable results between the two methods, proving that there are no measurable differences between the two experimental techniques. Additionally, no significant effects of the photocreated carriers are observed at these low power



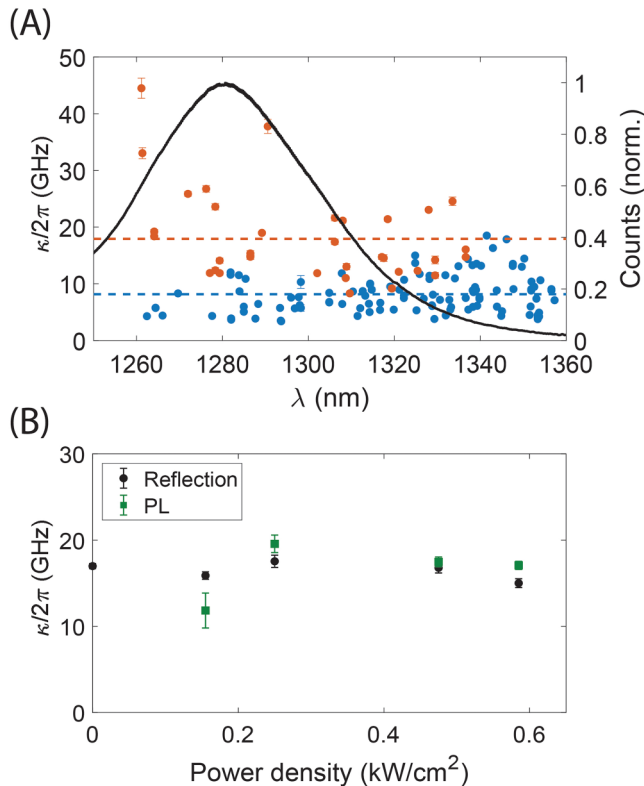


**FIG. 3.** (a) The red (blue) data points show the total loss rates (left axis) of the measured cavities fabricated in a wafer with (without) QDs. Error bars are derived from the Lorentzian fit of the reflection spectra. The dashed lines show the mean of the values with (red) and without (blue) QDs. In black: Normalized room temperature micro-PL spectrum of the QDs (right axis) as a reference, measured in an unpatterned area, at a power density of 1.5 kW/cm<sup>2</sup>. (b) Loss rate measured by PL (green) and reflection (black) for the same cavity with QDs, as a function of power density. The error bars are derived from the fit. The two measurements show comparable results for the two measurement methods.

densities. We conclude that PL is a suitable way to measure the quality factor of the cavities, if care is taken to deconvolve the instrument response function and if low pump power densities are used.

### C. Dependence on excitation density

To investigate the nature of the losses and whether they are saturable, we measured the cavity linewidth in a broad range of power densities and QD-cavity detuning, using the same 785 nm laser. While pumping, we performed both reflection and micro-PL measurements of the PhCCs. The measurements were carried out at increasing powers until reaching the saturation of the ground state of the QDs [Fig. 4(a)]. For this study, we selected cavities with resonant wavelengths located in three regions: blue-detuned, on resonance and red-detuned with respect to the ground state of the QDs [as shown in the inset of Fig. 4(c)]. As a control, analogous cavities are selected for the sample without QDs.

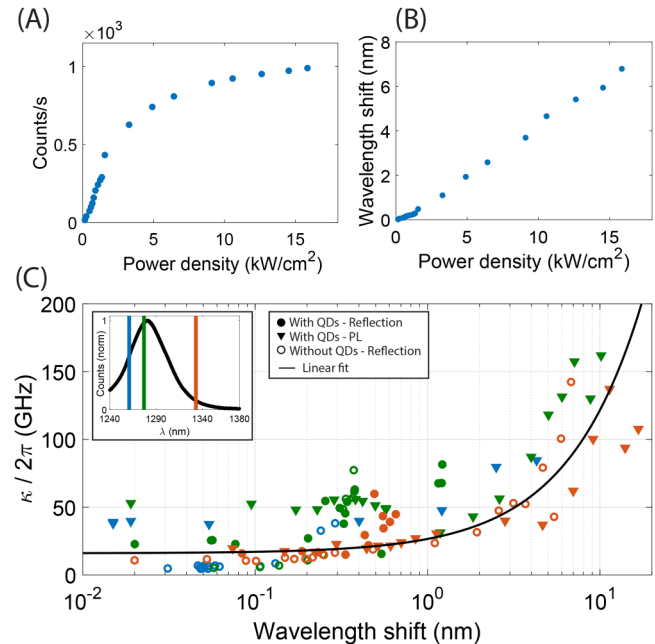


**FIG. 4.** (a) Peak of the QD ground state emission in an unpatterned area as a function of pump power density. (b) Wavelength shift of a cavity without QDs (nominal resonance at 1337 nm) at increasing pump power density. (c) Loss rate of the cavities with (full markers) and without QDs (empty markers) measured in reflection (circles) and PL (triangles) at increasing pump power. The solid line represents a linear fit, to show the expected trend from the free-carrier absorption. The colors of the datapoints refer to the cavity's detuning with respect to the QD emission at room temperature, plotted as black line in the inset: blue datapoints refer to blue-detuned cavities, green to cavities in resonance and red to red-detuned cavities.

The absorption of the pump in the nanobeam is influenced by the exact position of the laser spot, which may vary among different structures. In order to reliably compare measurements across different cavities, we use the thermal wavelength shift as a metric of the absorbed laser power. Indeed, we observed that the shift scales linearly with the laser power in this power range, as shown in Fig. 4(b).

The results of the study are shown in Fig. 4(c). For wavelength shifts < 0.1 nm, the measured loss rate is comparable to the one reported in Fig. 3(a), with a notable difference between samples with and without QDs, as already mentioned and commented above. At higher wavelength shifts, the loss rate of all the devices increases linearly, with a consistent trend for cavities with and without QDs, independently of their spectral alignment with the QD ground state emission. The lack of differences between the samples and the wavelength regions proves that the observed power dependence is not due to the presence of the QDs but can be attributed to the increased carrier density in the GaAs membrane. The linear dependence with the pump power density [linear fit is shown with the black solid line in Fig. 4(c)] suggests that the observed effect is given by FCA.<sup>26,27</sup>

04 March 2024 10:50:04

## IV. DISCUSSION

PhCCs with embedded QDs, commonly used to investigate exciton–photon coupling and lasing, have so far shown Qs significantly lower than their QD-free counterparts. This may in principle have different causes: (a) The different measurement method (PL vs reflection) used in some experiments; (b) The different wavelength range used (most experiments involving QDs are performed around 900–1000 nm, relatively close to the GaAs bandgap, making the cavities more sensitive to bandtail absorption); (c) Structural differences (e.g., surface roughness) related to the growth of the QDs; (d) Excitonic absorption from QD states or other absorption intrinsically related to the QDs. In Ref. 18, a strong improvement of the quality factor was observed for PhCCs with QDs at resonant wavelengths around 950 nm, upon surface passivation using a standard sulfur-based GaAs-passivation method. This was attributed to the passivation of surface defects and correspondingly a reduction of their absorption. In Ref. 19, sulfur-passivation followed by deposition of a thin Al<sub>2</sub>O<sub>3</sub> layer was observed to significantly reduce the optical loss in an open planar GaAs microcavity operating around 920 nm. The observed passivation effect was in this case explained by the reduction of the surface electric field and correspondingly of band bending and bandtail absorption. Both these reports point in the direction of surface-related effects on the absorption of the bulk GaAs—unrelated to the presence of QDs. These effects are indeed expected to be more prominent for wavelengths close to the GaAs absorption edge. On the basis of these results, and of the extensive literature on high-Q PhCCs in the telecom (1300–1550 nm) wavelength range, one would expect that high-Q PhCCs with QDs could be fabricated at telecom wavelengths, where the effect of the GaAs bandtail is expected to be negligible. Our study is complementary to these previous reports and shades new light on absorption processes intrinsically related to the QDs. We evidence a clear difference between the optical loss rates in nominally identical cavities with and without QDs, fabricated with an identical fabrication process, and resonant in the same wavelength range, > 400 meV apart from the GaAs band edge. Our systematic approach allows us to directly exclude some of the possible causes for additional loss mentioned above:

- We show that PL and reflection measurements provide the same loss values, if proper care is taken to minimize the pump power density and to deconvolve the instrument response function of the spectrometer. At higher pump powers, we observe a clear broadening of the lines, due to free-carrier absorption.
- We clearly identify additional loss in QD-containing structures with respect to identical QD-free structures having resonant wavelengths in the same range. This is the first unequivocal proof of the effect of the QDs on the loss, unrelated to surfaces (which are the same in both samples).
- As we use samples with comparable surface roughness and the same fabrication process, we can reasonably exclude that the observed loss difference is due to structural differences—this point is further discussed below.
- By systematically studying the loss as a function of detuning and pump power density, we can exclude direct excitonic absorption as the source of QD-related loss. Other potential absorption channels are discussed below. While this brings

solid evidence and valuable information on additional losses in PhCCs embedding QDs, the question of their physical origin still remains open. In the following we analyze several mechanisms which could explain our observations.

## A. Scattering due to surface roughness or composition inhomogeneity

For the sample with QDs, we reported the presence of shallow mounds aligned along [110]. The low profile of such mounds (approximately 3.8 nm for the maximum peak-to-valley) resulting in low  $R_q$ , as well as their large dimensions ( $\sim 3 \mu\text{m} \times 1 \mu\text{m}$ , much bigger than the mode volume of our structures) let us conclude that their impact on the Q of the devices is not predominant. We also looked at the small roughness [insets of Figs. 1(d) and 1(e)] and simulated its impact following the steps of Ref. 28, obtaining a loss rate associated with the surface roughness of  $\sim 0.2$  GHz, two orders of magnitude lower than the losses measured in the samples. We also investigated whether the composition inhomogeneity related to the QDs could lead to Rayleigh scattering in the cavity. We approach the problem by treating the QDs as small InAs spheres with a diameter of 10 nm surrounded in GaAs. Then, we estimated the Rayleigh scattering cross section as<sup>29</sup>

$$\sigma_R = \frac{8\pi}{3} (2\pi n_{\text{GaAs}})^4 \left( \frac{a^6}{\lambda^4} \right) \left( \frac{m^2 - 1}{m^2 + 1} \right)^2, \quad (1)$$

where  $n_{\text{GaAs}}$  is the refractive index of GaAs,  $a$  the radius of the QD particle,  $\lambda$  the wavelength, and  $m$  the ratio between the refractive index of InAs and the refractive index of GaAs. From the cross section we evaluate the absorption coefficient  $\alpha_R = 0.034 \text{ m}^{-1}$  of the QD layer, which is then used to compute the Q with COMSOL Multiphysics. The simulated loss rate is  $\kappa_R = 30 \text{ kHz}$ , several orders of magnitude smaller than the measured difference between the samples with and without QDs.

## B. Intrinsic absorption losses

As we exclude the role of scattering and absorption from surface states (as these are the same for the two samples), we must conclude that the observed additional loss is related to QD-related absorption processes. From the wavelength dependence of the loss we can already exclude direct excitonic absorption from the QDs as relevant loss channel, as it would be relevant only for cavities on resonance with the QD emission and be strongly reduced for red-detuned cavities. We support this statement also by showing that the loss rate does not saturate with increasing pump power, as would be expected from direct inter-band absorption of QDs in the presence of strong pump power that saturates the QDs ground state.

A possible origin of the loss, which is compatible with our experimental observations, is the absorption by unsaturable midgap trap states that originate from the growth. Several works<sup>30–32</sup> report the presence of deep trap states in In(Ga)As/GaAs QDs tuned to the near-infrared. Particularly, very similar structures have been characterized with time-resolved PL suggesting the existence of nonradiative traps in the In(Ga)As matrix in the close vicinity of the QDs.<sup>33</sup> Our measurements allow estimating an upper limit to

04 March 2024 10:50:04

the density of such trap states. To do so, we make use of Ref. 34 where a complete set of eleven deep trap states with activation energy spanning between 0.15 and 0.58 eV and cross section between  $10^{-18}$  and  $10^{-15}$  cm<sup>2</sup> was reported. Our study does not allow us to distinguish between the contribution of each state, also because none of them would produce a spectral resonance in the region of interest. However, assuming that the highest cross section has the most effect—we can estimate the surface density of trap states as being  $\sim 750 \mu\text{m}^{-2}$ . We cannot pinpoint how these states originate during the growth process, as well as their dependence on the QD density. In fact, they can also be due to defects in the wetting layer.

We would like to point out that at higher QD density also other loss mechanisms might become relevant. Indeed, previous fabrication efforts (data not reported in this work) have shown that the surface roughness is highly impacted when the QD density approaches  $\sim 300 \mu\text{m}^{-2}$ , with the surface RMS being four times higher than that of the control wafer without QDs, and valley-to-peak mounds of about 15 nm high.

Our experimental results indicate that a thorough understanding of defects in QD growth is needed to minimize not only nonradiative carrier recombination but also optical loss in nanophotonic QD devices. Possible avenues include the further optimization of the growth temperature and of the capping procedure. Additionally, it would be interesting to investigate the excess optical loss in cavities embedding QDs, grown by other methods, such as droplet epitaxy<sup>35</sup> and site-controlled growth.<sup>36</sup>

## V. CONCLUSION

We presented a systematic investigation of the optical loss in PhCCs with and without self-embedded In(Ga)As/GaAs QDs with ground state emission tuned to  $\sim 1.3 \mu\text{m}$ . The growth has been optimized to reduce the QD-induced surface roughness, leading to a comparable surface roughness between the wafer without and with QDs.

Our study has unequivocally identified an additional loss channel for the PhCCs with emitters compared to their passive counterparts, independently of the measurement technique and resonance wavelength. By performing simultaneous measurements in reflection and PL at increasing pump powers, we conclude that such losses—about  $(\bar{\kappa}_{\text{QD}} - \bar{\kappa}_{\text{noQD}})/2\pi \approx 7$  GHz, which corresponds to an upper limit of  $Q \approx 3.3 \times 10^4$ —are not related to direct excitonic absorption. A possible origin that is compatible with our experimental data is that the measured loss could instead be due to mid-band traps that arise from the QD growth.

We note that such excess loss does not represent a limiting factor in the context of QDs PhCC nanolasers, where devices with  $Q$  as low as 1130<sup>7</sup> have been reported. In the context of single-photon devices based on QDs, the reported loss rate does not affect the operation in the weak-coupling regime (e.g., as single-photon source<sup>37</sup>), but impacts the possibility of coherent excitation swap between an exciton in the QD and a photon in the cavity. Here, increasing  $Q$  of the PhCCs would increase the quantum cooperativity of the devices, thus reducing the decoherence of the quantum states.

We believe that our research will stimulate the development of high- $Q$  nanophotonic devices, underscoring the potential for future progress and applications.

## ACKNOWLEDGMENTS

The authors thank Professor Vincenzo Savona École polytechnique fédérale de Lausanne for initially proposing the investigation of losses in PhCCs with embedded QDs, Pierre Busi (TU/e) for his contribution to the design of PhCCs, Menno Jansen (TU/e) for his contribution to the experimental methods and dr. Francesco Pagliano (nanoPHAB b.v.) for developing the fabrication recipe used in this work. The authors acknowledge useful discussions with R. Burgwal.

This research was funded by Netherlands Organization for Scientific Research (NWO/OCW), as part of the Vrij Programma (Grant No. 680-92-18-04) grant and of the Zwaartekracht Research Center for Integrated Nanophotonics (Grant No. 024.002.033)

## AUTHOR DECLARATIONS

### Conflict of Interest

The authors have no conflicts to disclose.

### Author Contributions

**Matteo Lodde:** Data curation (equal); Formal analysis (equal); Methodology (equal); Resources (equal); Visualization (equal); Writing – original draft (equal); Writing – review & editing (equal). **Rene P. J. van Veldhoven:** Resources (equal); Writing – review & editing (supporting). **Ewold Verhagen:** Funding acquisition (equal); Supervision (equal); Writing – review & editing (equal). **Andrea Fiore:** Conceptualization (equal); Funding acquisition (equal); Supervision (equal); Writing – original draft (equal); Writing – review & editing (equal).

## DATA AVAILABILITY

The data that support the findings of this study are available from the corresponding author upon reasonable request.

## REFERENCES

- J. Chan, T. P. Alegre, A. H. Safavi-Naeini, J. T. Hill, A. Krause, S. Gröblacher, M. Aspelmeyer, and O. Painter, “Laser cooling of a nanomechanical oscillator into its quantum ground state,” *Nature* **478**, 89–92 (2011).
- H. Benisty, S. Combrié, A. D. Rossi, and Q. V. Tran, “GaAs photonic crystal cavity with ultrahigh Q: Microwatt nonlinearity at  $1.55 \mu\text{m}$ ,” *Opt. Lett.* **33**, 1908–1910 (2008).
- H. Okada, M. Fujimoto, N. Tanaka, Y. Saito, T. Asano, S. Noda, S. Noda, S. Noda, Y. Takahashi, and Y. Takahashi, “ $1.2\text{-}\mu\text{m}$ -band ultrahigh-Q photonic crystal nanocavities and their potential for Raman silicon lasers,” *Opt. Express* **29**, 24396–24410 (2021).
- T. Asano, Y. Ochi, Y. Takahashi, K. Kishimoto, S. Noda, R. D. Meade, A. Devenyi, J. D. Joannopoulos, O. L. Alerhand, D. A. Smith, K. Kash, O. Painter, R. K. Lee, A. Scherer, A. Yariv, P. D. Dapkus, and I. Kim, “Photonic crystal nanocavity with a Q factor exceeding eleven million,” *Opt. Express* **25**, 1769–1777 (2017).
- P. Seidler, K. Lister, U. Drechsler, J. Hofrichter, T. Stöferle, K. Takeda, T. Sato, A. Shinya, K. Nozaki, W. Kobayashi, H. Taniyama, M. Notomi, K. Hasebe, T. Kakitsuka, S. Matsuo, B. Schmidt, Q. Xu, J. Shakya, S. Manipatruni, M. Lipson, D. J. Ripin, K. Y. Lim, G. S. Petrich, P. R. Villeneuve, S. Fan, E. R. Thoen, J. D. Joannopoulos, E. P. Ippen, L. A. Kolodziejski, P. B. Deotare, M. W. McCutcheon, I. W. Frank, M. Khan, and M. Lončar, “Slotted photonic crystal nanobeam cavity with an ultrahigh quality factor-to-mode volume ratio,” *Opt. Express* **21**, 32468–32483 (2013).



- <sup>6</sup>O. Painter, R. K. Lee, A. Scherer, A. Yariv, J. D. O'Brien, P. D. Dapkus, and I. Kim, "Two-dimensional photonic band-gap defect mode laser," *Science* **284**, 1819–1821 (1999).
- <sup>7</sup>B. Ellis, M. A. Mayer, G. Shambat, T. Sarmiento, J. Harris, E. E. Haller, J. Vučković, and V. Vučković, "Ultralow-threshold electrically pumped quantum-dot photonic-crystal nanocavity laser," *Nat. Photonics* **5**, 297–300 (2011).
- <sup>8</sup>J. Vučković, D. Fattal, C. Santori, G. S. Solomon, and Y. Yamamoto, "Enhanced single-photon emission from a quantum dot in a micropost microcavity," *Appl. Phys. Lett.* **82**, 3596–3598 (2003).
- <sup>9</sup>P. Michler, A. Kiraz, C. Becher, W. V. Schoenfeld, P. M. Petroff, L. Zhang, E. Hu, and A. Imamoglu, "A quantum dot single-photon turnstile device," *Science* **290**, 2282–2285 (2000).
- <sup>10</sup>A. Faraon, I. Fushman, D. Englund, N. Stoltz, P. Petroff, and J. Vučković, "Coherent generation of non-classical light on a chip via photon-induced tunneling and blockade," *Nat. Phys.* **4**(11), 859–863 (2008).
- <sup>11</sup>M. Petruzzella, F. M. Pagliano, Ž. Zobenica, S. Birindelli, M. Cotrufo, F. W. M. van Otten, R. W. van der Heijden, and A. Fiore, "Electrically driven quantum light emission in electromechanically tuneable photonic crystal cavities," *Appl. Phys. Lett.* **111**, 251101 (2017).
- <sup>12</sup>L. Bremer, S. Rodt, S. Reitzenstein, X. Wu, A. Kolar, J. Chung, and P. Lodahl, "Quantum-dot based photonic quantum networks," *Quantum Sci. Technol.* **3**, 013001 (2017).
- <sup>13</sup>H. Kim, R. Bose, T. C. Shen, G. S. Solomon, and E. Waks, "A quantum logic gate between a solid-state quantum bit and a photon," *Nat. Photonics* **7**(5), 373–377 (2013).
- <sup>14</sup>T. Volz, A. Reinhard, M. Winger, A. Badolato, K. J. Hennessy, E. L. Hu, and A. Imamoglu, "Ultrafast all-optical switching by single photons," *Nat. Photonics* **6**(9), 605–609 (2012).
- <sup>15</sup>J. Vučković and Y. Yamamoto, "Photonic crystal microcavities for cavity quantum electrodynamics with a single quantum dot," *Appl. Phys. Lett.* **82**, 2374–2376 (2003).
- <sup>16</sup>Y. Ota, D. Takamiya, R. Ohta, H. Takagi, N. Kumagai, S. Iwamoto, and Y. Arakawa, "Large vacuum Rabi splitting between a single quantum dot and an H0 photonic crystal nanocavity," *Appl. Phys. Lett.* **112**, 93101 (2018).
- <sup>17</sup>P. Boucaud, Y. Campidelli, N. Zerounian, D. Bensahel, O. Kermarrec, M. E. Kurdi, X. Checoury, S. David, and T. P. Ngo, "Quality factor of Si-based photonic crystal L3 nanocavities probed with an internal source," *Opt. Express* **16**(12), 8780–8791 (2008).
- <sup>18</sup>K. Kuruma, Y. Ota, M. Kakuda, S. Iwamoto, and Y. Arakawa, "Surface-passivated high-Q GaAs photonic crystal nanocavity with quantum dots," *APL Photonics* **5**, 046106 (2020).
- <sup>19</sup>D. Najer, N. Tömm, A. Javadi, A. R. Korsch, B. Petrak, D. Riedel, V. Dolique, S. R. Valentin, R. Schott, A. D. Wieck, A. Ludwig, and R. J. Warburton, "Suppression of surface-related loss in a gated semiconductor microcavity," *Phys. Rev. Appl.* **15**, 044004 (2021).
- <sup>20</sup>L. Balet, M. Francardi, A. Gerardino, N. Chauvin, B. Alloing, C. Zinoni, C. Monat, L. H. Li, N. L. Thomas, R. Houdré, and A. Fiore, "Enhanced spontaneous emission rate from single InAs quantum dots in a photonic crystal nanocavity at telecom wavelengths," *Appl. Phys. Lett.* **91**, 123115 (2007).
- <sup>21</sup>G. Kiršanskė, H. Thyrrestrup, R. S. Daveau, C. L. Dreeßen, T. Pregnotato, L. Midolo, P. Tighineanu, A. Javadi, S. Stobbe, R. Schott, A. Ludwig, A. D. Wieck, S. I. Park, J. D. Song, A. V. Kuhlmann, I. Söllner, M. C. Löbl, R. J. Warburton, and P. Lodahl, "Indistinguishable and efficient single photons from a quantum dot in a planar nanobeam waveguide," *Phys. Rev. B* **96**, 165306 (2017).
- <sup>22</sup>J. X. Chen, A. Markus, A. Fiore, U. Oesterle, R. P. Stanley, J. F. Carlin, R. Houdré, M. Ilegems, L. Lazzarini, L. Nasi, M. T. Todaro, E. Piscopiello, R. Cingolani, M. Catalano, J. Katcki, J. Ratajczak, A. Markus, A. Fiore, U. Oesterle, R. P. Stanley, J. F. Carlin, R. Houdré, M. Ilegems, L. Lazzarini, L. Nasi, M. T. Todaro, E. Piscopiello, R. Cingolani, M. Catalano, J. Katcki, and J. Ratajczak, "Tuning InAs/GaAs quantum dot properties under Stranski-Krastanov growth mode for 1.3  $\mu\text{m}$  applications," *J. Appl. Phys.* **91**, 6710–6716 (2002).
- <sup>23</sup>L. Wang, A. Rastelli, and O. G. Schmidt, "Structural and optical properties of In(Ga)As/GaAs quantum dots treated by partial capping and annealing," *J. Appl. Phys.* **100**, 64313 (2006).
- <sup>24</sup>M. Lipson and V. R. Almeida, "Optical bistability on a silicon chip," *Opt. Lett.* **29**(20), 2387–2389 (2004).
- <sup>25</sup>M. Aspelmeyer, T. J. Kippenberg, and F. Marquardt, "Cavity optomechanics," *Rev. Mod. Phys.* **86**, 1391–1452 (2014).
- <sup>26</sup>W. Walukiewicz, L. Lagowski, L. Jastrzebski, M. Lichtensteiger, and H. C. Gatos, "Electron mobility and free-carrier absorption in GaAs: Determination of the compensation ratio," *J. Appl. Phys.* **50**, 899–908 (1979).
- <sup>27</sup>D. K. Schroder, R. N. Thomas, and J. C. Swartz, "Free carrier absorption in silicon," *IEEE J. Solid-State Circuits* **13**, 180–187 (1978).
- <sup>28</sup>K. K. Lee, D. R. Lim, H. C. Luan, A. Agarwal, J. Foresi, and L. C. Kimerling, "Effect of size and roughness on light transmission in a Si/SiO<sub>2</sub> waveguide: Experiments and model," *Appl. Phys. Lett.* **77**, 1617–1619 (2000).
- <sup>29</sup>A. J. Cox, A. J. DeWeerd, and J. Linden, "An experiment to measure Mie and Rayleigh total scattering cross sections," *Am. J. Phys.* **70**, 620–625 (2002).
- <sup>30</sup>S. Golovynskyi, O. I. Datsenko, L. Seravalli, G. Trevisi, P. Frigeri, I. S. Babichuk, I. Golovynska, B. Li, and J. Qu, "Defect influence on in-plane photocurrent of InAs/InGaAs quantum dot array: Long-term electron trapping and Coulomb screening," *Nanotechnology* **30**, 305701 (2019).
- <sup>31</sup>D. Sreenivasan, J. E. Haverkort, T. J. Eijkemans, and R. Nötzel, "Photoluminescence from low temperature grown InAs/GaAs quantum dots," *Appl. Phys. Lett.* **90**, 112109 (2007).
- <sup>32</sup>S. Golovynskyi, O. Datsenko, L. Seravalli, O. Kozak, G. Trevisi, P. Frigeri, I. S. Babichuk, I. Golovynska, and J. Qu, "Deep levels in metamorphic InAs/InGaAs quantum dot structures with different composition of the embedding layers," *Semicond. Sci. Technol.* **32**, 125001 (2017).
- <sup>33</sup>A. Fiore, P. Borri, W. Langbein, J. M. Hvam, U. Oesterle, R. Houdré, R. P. Stanley, and M. Ilegems, "Time-resolved optical characterization of InAs/InGaAs quantum dots emitting at 1.3  $\mu\text{m}$ ," *Appl. Phys. Lett.* **76**, 3430–3432 (2000).
- <sup>34</sup>M. Pavlović, U. V. Desnica, J. Gladić, M. PavlovićPavlović, and J. Gladić, "Complete set of deep traps in semi-insulating GaAs," *J. Appl. Phys.* **88**, 4563–4570 (2000).
- <sup>35</sup>M. Gurioli, Z. Wang, A. Rastelli, T. Kuroda, and S. Sanguinetti, "Droplet epitaxy of semiconductor nanostructures for quantum photonic devices," *Nat. Mater.* **18**(8), 799–810 (2019).
- <sup>36</sup>M. H. Baier, E. Pelucchi, E. Kapon, S. Varoutsis, M. Gallart, I. Robert-Philip, and I. Abram, "Single photon emission from site-controlled pyramidal quantum dots," *Appl. Phys. Lett.* **84**, 648–650 (2004).
- <sup>37</sup>P. Lodahl, S. Mahmoodian, and S. Stobbe, "Interfacing single photons and single quantum dots with photonic nanostructures," *Rev. Mod. Phys.* **87**, 347–400 (2015).